NASA Technical Memorandum 105160
AIAA-91-2013

Verification of the Proteus Two-Dimensional Navier-Stokes Code for Flat Plate and Pipe Flows

Julianne M. Conley
Lewis Research Center
Cleveland, Ohio

and

Patrick L. Zeman
Arnold Engineering and Development Center
Arnold AFB, Tennessee

Prepared for the
27th Joint Propulsion Conference
cosponsored by AIAA, SAE, ASME, and ASEE
Sacramento, California, June 24-27, 1991

VERIFICATION OF THE PROTEUS TWO-DIMENSIONAL NAVIER-STOKES CODE FOR FLAT PLATE AND PIPE FLOWS

Julianne M. Conley*
National Aeronautics and Space Administration
Lewis Research Center
Cleveland, Ohio

Patrick L. Zeman
Arnold Engineering and Development Center
Arnold AFB, Tennesee

Abstract

The Proteus Navier-Stokes Code is evaluated for two-dimensional/axisymmetric, viscous, incompressible, internal and external flows. The particular cases to be discussed are laminar and turbulent flows over a flat plate, laminar and turbulent developing pipe flows and turbulent pipe flow with swirl. Results are compared with exact solutions, empirical correlations and experimental data. A detailed description of the code set-up, including boundary conditions, initial conditions, grid size and grid packing is given for each case.

Introduction

An effort is underway at the NASA Lewis Research Center to develop a two and three-dimensional Navier-Stokes code, called Proteus, for aerospace propulsion applications.(1) The emphasis in this effort is not algorithm development or research on numerical methods, but on the development of the code itself. The objective is to develop a code that is user-oriented, easily modified, and well documented. Code readability, modularity, and both internal and external documentation have been emphasized.

Proteus solves the Reynolds-averaged, unsteady, compressible Navier-Stokes equations in strong conservation law form. Turbulence is modeled using a Baldwin-Lomax(2) based algebraic eddy viscosity model . The governing equations are written in Cartesian coordinates and transformed into generalized nonorthogonal body-fitted coordinates. They are solved by marching in time using a fully-coupled alternating direction implicit solution procedure with generalized first or second order time differencing.(3-4) The boundary conditions are also treated implicitly, and may be steady or unsteady. All terms, including the diffusion terms, are linearized using second order Taylor series expansions.

Two versions of the Proteus code exist: one for two-dimensional planar and axisymmetric flow, and one for three-dimensional flow. In addition to solving the full time-averaged Navier-Stokes equations, Proteus includes options to solve the thin-layer or Euler equations, and to eliminate the energy equation by assuming constant stagnation enthalpy. Artificial viscosity is used to minimize the odd-even decoupling resulting from the use of central spatial differencing for the convective terms, and to control pre- and post-shock oscillations in supersonic flow. Two artificial viscosity models are available -- a combination implicit/explicit constant coefficient model (5), and an explicit nonlinear coefficient model designed specifically for flows with shock waves.(6-7). At the NASA Lewis Research Center, the code is typically run either on the CRAY X-MP or the CRAY Y-MP computer, and is highly vectorized.

*Aerospace Engineer
Member AIAA

In order to assess the code's validity for calculating fundamental fluid flows encountered in most aerospace propulsion applications, a series of validation cases have been run, using the two-dimensional planar/axisymmetric version of the code. These cases are for both internal and external incompressible flows. This paper describes validation studies for laminar and turbulent flat plate boundary layers with zero pressure gradient, and for laminar and turbulent developing pipe flows and turbulent pipe flow with swirl. Incompressible cases in Proteus were simulated by running at a Mach number between 0.1 and 0.3. In the results for both flat plate and pipe flow to be presented, constant total enthalpy was assumed, and the energy equation was not solved.

Test Cases

Laminar Flat Plate Flow

Incompressible laminar flow over a flat plate with zero pressure gradient can be compared with the exact solution of Blasius.(8) The results of one such comparison are shown in Figures 2-6, plotted with the results of Blasius. For this test case, the freestream Mach number was 0.2 and Re_x, the Reynolds number based on x, ranged from 20,000 at the upstream computational boundary to 100,000 at the downstream computational boundary. A 201x101 grid was used, with packing in the vertical direction near the plate surface such that the ratio of the minimum to maximum cell height, defined as the packing ratio, was 0.05; the grid was uniform in the x-direction. The grid extended horizontally from $x/L = 0.25$ to $x/L = 1.25$ and vertically from $y/L = 0.0$ to $y/L = 0.05$, where L is a reference length used by Proteus to normalize input values. For this test case, $L \approx 52\delta_{max}$, where δ_{max} is the maximum boundary layer thickness. A portion of the grid extending from $x/L = 0.25$ to $x/L = 0.29$ is illustrated in Figure 1. For the initial conditions, u, the horizontal x-velocity, and v, the vertical y-velocity, were computed using the Blasius solution. The static pressure, p, was set to p_∞, the freestream static pressure, everywhere. For the boundary conditions, at the upstream boundary, p, u and v were held at the initial condition values. At the downstream boundary, $p = p_\infty$, and $\partial^2 u/\partial x^2 = \partial^2 v/\partial x^2 = 0$. At the surface, $\partial p/\partial y = 0$, and $u = v = 0$. At the freestream boundary, $p = p_\infty$, $u = u_\infty$ and $\partial v/\partial y = 0$.

The results shown in Figures 2-6 were obtained after 4100 iterations. Figure 2 shows the x-velocity profile plotted against the Blasius similarity coordinate, η, where

$$\eta = y\sqrt{u_\infty / \nu x}$$

with ν as the kinematic viscosity. Here, the Proteus results are indistinguishable from the Blasius profile, indicating excellent performance by Proteus. In the y-velocity profile of Figure 3, the Blasius results are also indistinguishable from the Proteus

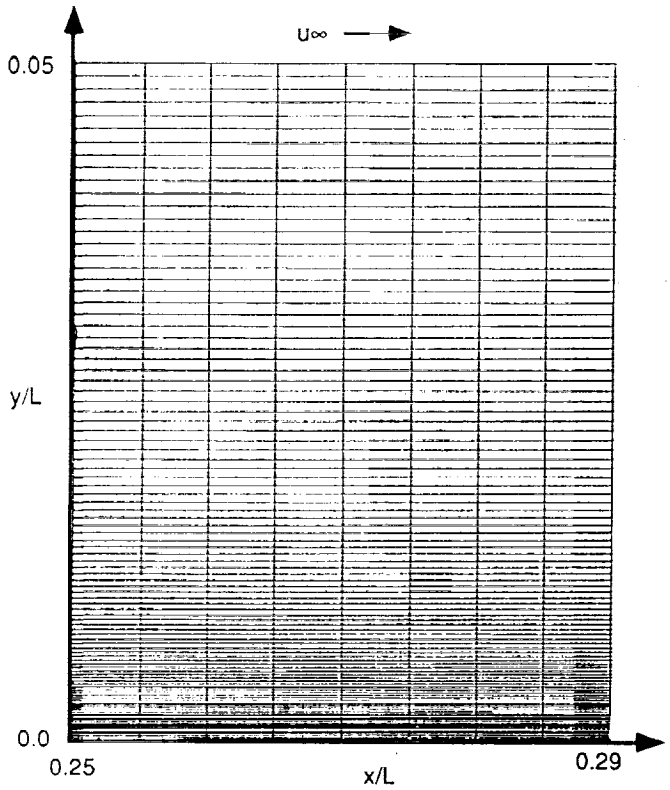

Fig. 1 A portion of the grid used for laminar flat plate calculations.

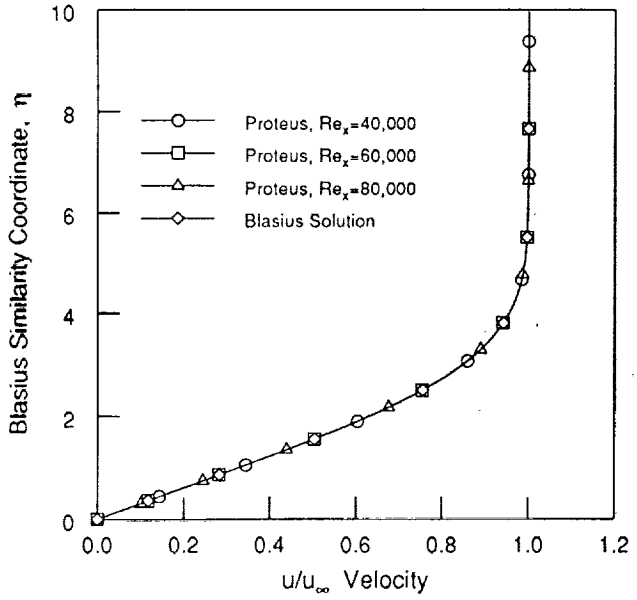

Fig. 2. X-velocity profiles for laminar flat plate flow.

results. Figure 4 shows the local skin friction coefficient plotted against Re_θ, the Reynolds number based on θ, the momentum thickness. Figure 5 shows θ versus x and Figure 6 shows the displacement thickness, δ^*, versus x. Figures 4 through 6 all exhibit excellent agreement between the Proteus results and the Blasius solution. Thus, Proteus is capable of accurately calculating incompressible laminar flow over a flat plate.

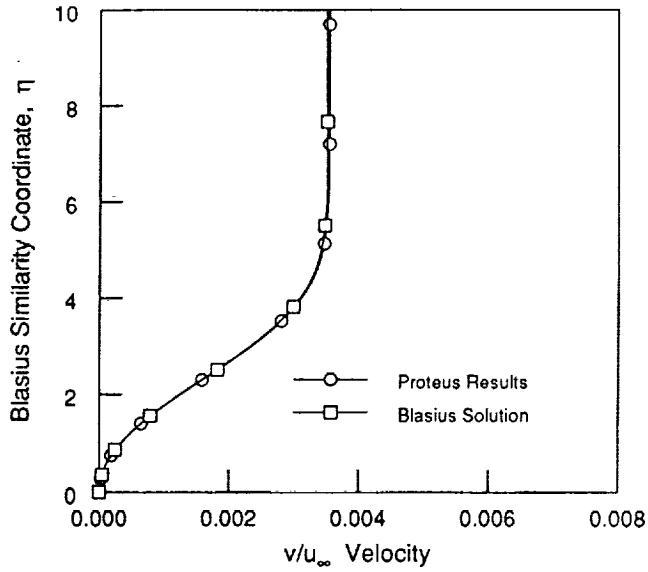

Fig. 3. Y-velocity profile for laminar flat plate flow.

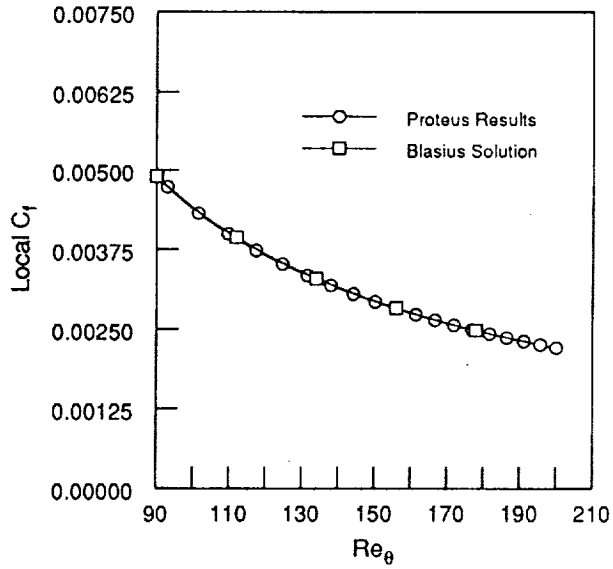

Fig. 4. Local skin friction coefficient for laminar flat plate flow.

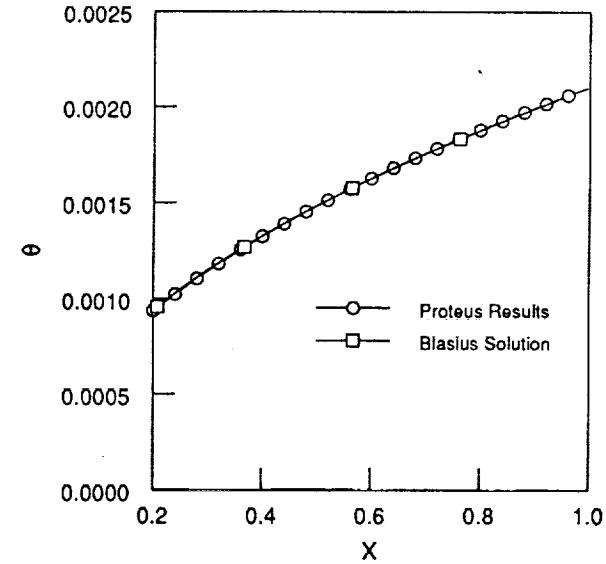

Fig. 5. Momentum thickness for laminar flat plate flow.

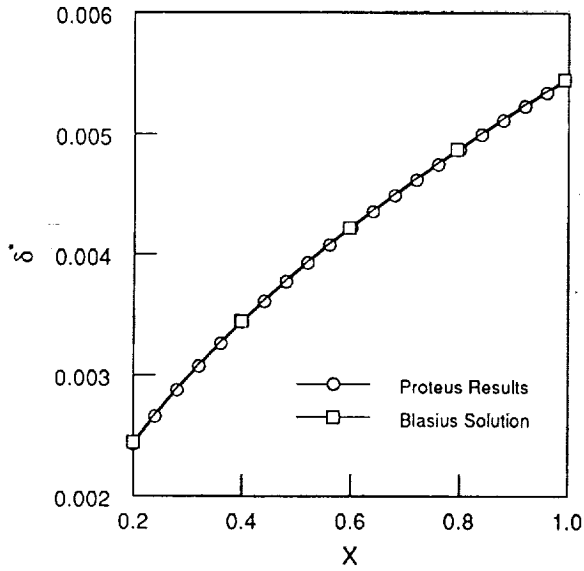

Fig. 6. Displacement thickness for laminar flat plate flow.

A study was done to minimize the number of grid points in the streamwise and normal directions required to accurately compute the above described laminar flow. The results of this study are shown in Figures 7 and 8. In Figures 7a-7d, the number of streamwise grid points is decreased from 101 to 13 points, while the number of normal grid points is held constant at 101. The results begin to deviate from the Blasius solution below 26 points, as shown in the deviation of the 13x101 curve of Figure 7d. This shows that a minimum of 26 streamwise grid points are required for an accurate solution. In Figures 8a-8c, 26 grid points are used in the streamwise direction, and the number of grid points in the normal direction is decreased from 101 to 26 points. The results begin to disagree with the Blasius curve when fewer than 51 points are used, as seen by the deviation in the 26x26 curve of Figure 8c. Thus, the smallest grid needed to accurately calculate this laminar flow over a flat plate is a 26x51 grid.

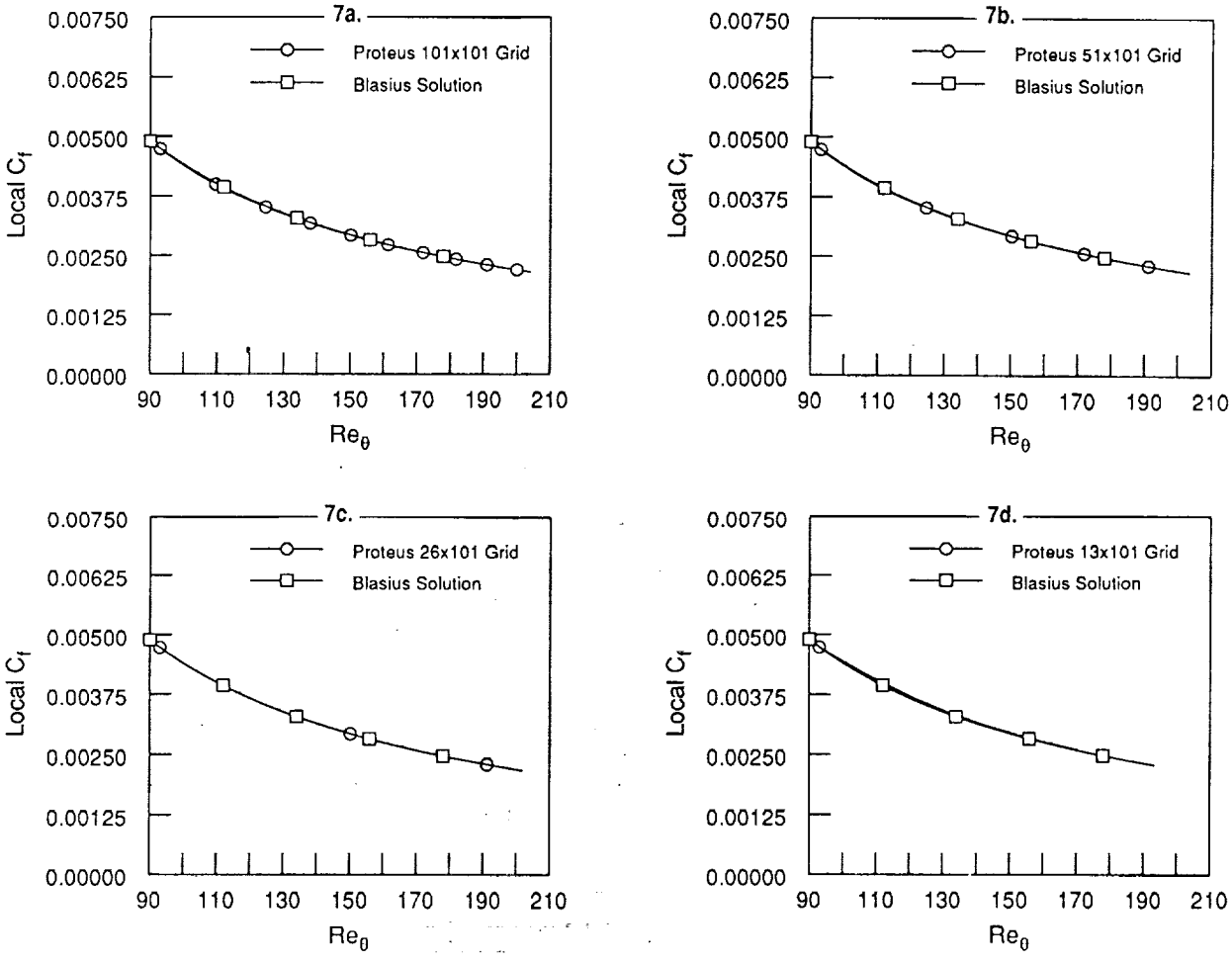

Fig. 7a-d. Variation in the number of streamwise grid points.

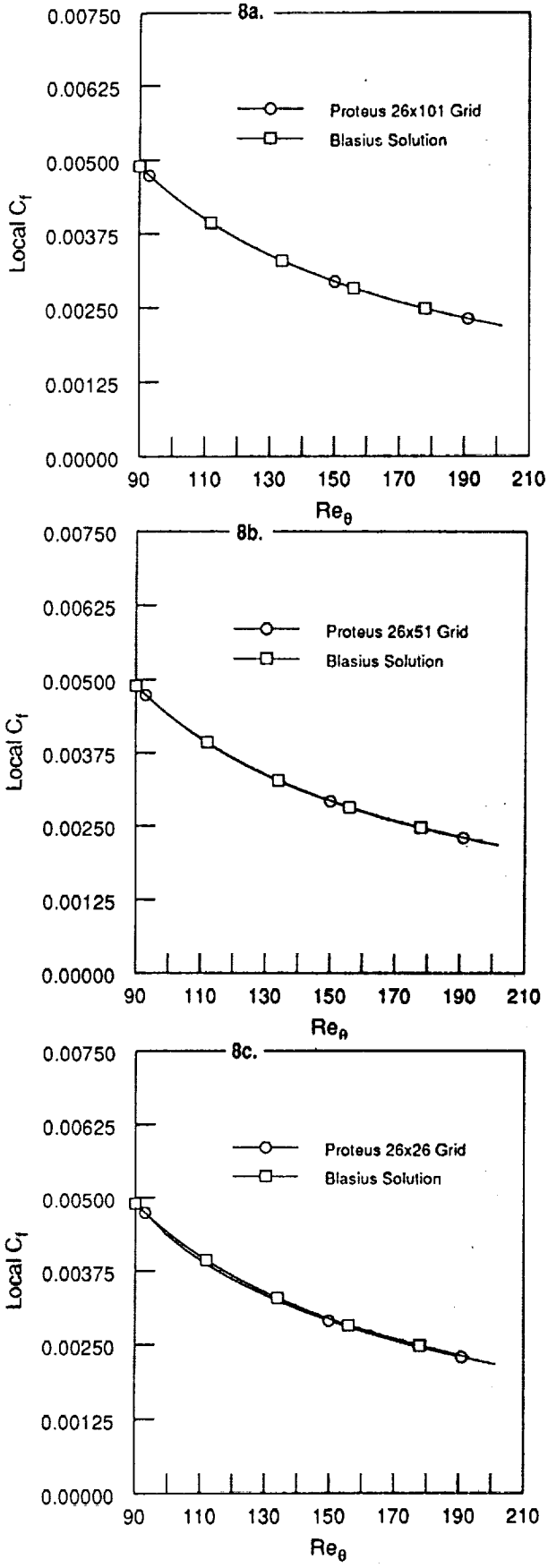

Fig. 8a-c. Variation in the number of normal grid points.

Turbulent Flat Plate Flow

Results for incompressible turbulent flow over a flat plate are shown in Figures 9-11. For the cases shown, the freestream Mach number was 0.2 and Re_x ranged from 4,000,000 at the upstream computational boundary to 16,000,000 at the downstream boundary. A 101x191 grid was used with packing in the vertical direction at the plate surface such that the packing ratio was 0.005. Grid packing was also used in the x-direction at the upstream boundary such that the packing ratio was 0.05. The grid extended from x/L = 0.33 to x/L = 1.33 and from y/L = 0.0 to y/L = 0.048, where $L \approx 58\delta_{max}$. For the initial conditions, u was determined from an expression developed by Musker[9], with v = 0, and $p = p_\infty$. The boundary conditions were identical to those for the laminar flat plate case.

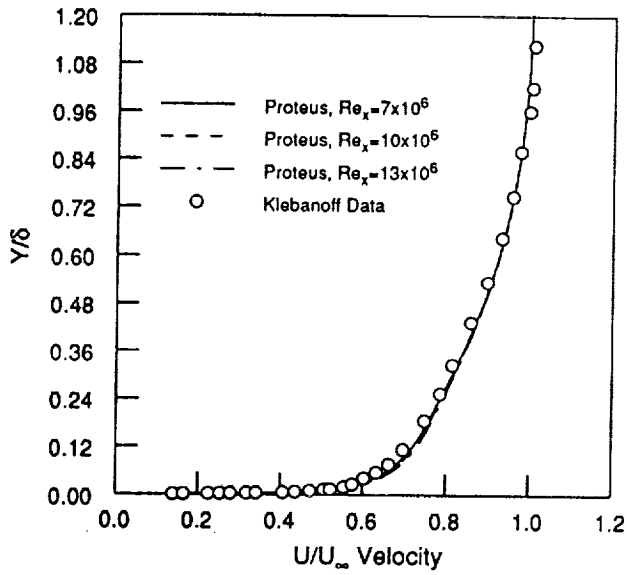

Fig. 9. X-Velocity profiles for turbulent flat plate flow.

Figure 9 shows the x-velocity plotted with y/δ, where δ is the boundary layer thickness. Note that the Proteus results at the three different Reynolds numbers shown are each represented by a curve and agree so closely that it is difficult to distinguish them on the plot. This is to be expected since the profiles are plotted with similarity coordinates. The results also show good agreement with the experimental data of Klebanoff.[10] Figure 10 shows the same Proteus results plotted on a semi-log graph with u^+ and y^+ coordinates, where $u^+ = u/u_\tau$, with u_τ equal to the shear velocity, and $y^+ = yu_\tau/\nu$. These results show good agreement with the law of the wall correlation.[11] Figure 11 shows a plot of the local skin friction coefficient, c_f, versus Re_θ, compared with the Karman-Schoenherr correlation[12] and the experimental data of Weighardt.[13] Notice that the Proteus results exhibit a drop in c_f at the upstream boundary, where Re_x = 4,000,000 or Re_θ = 6,500 with the remaining portion of the curve in agreement with the data of References 14 and 15. This drop at the upstream boundary is most likely a result of using an inexact boundary condition at this boundary. Recall that at the upstream boundary, a u-profile was approximated and v was set to zero. Other upstream boundary conditions were also

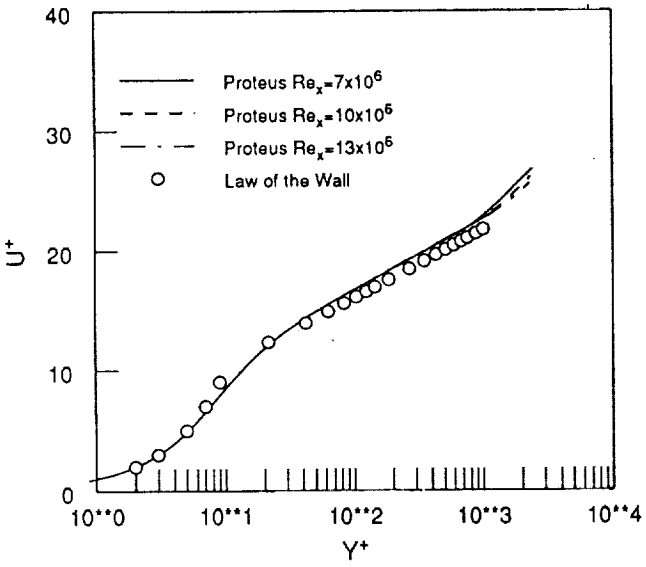

Fig. 10. X-Velocity profiles for turbulent flat plate flow.

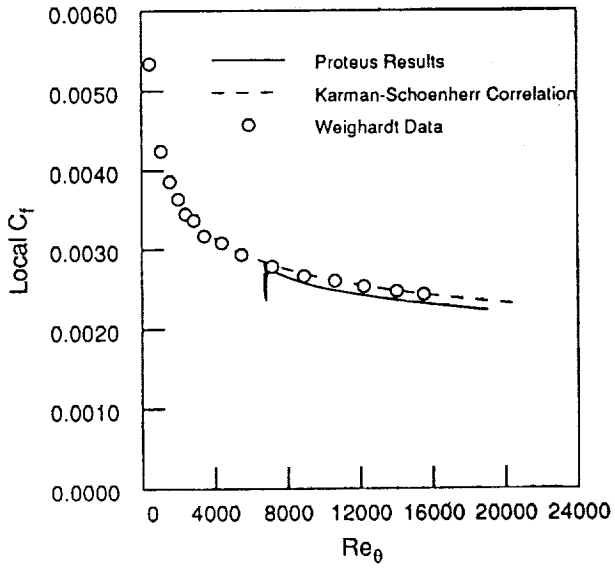

Fig. 11. Local skin friction coefficient for turbulent flat plate flow.

considered, such as using a u-profile computed from the Musker expression and v either computed from the continuity equation or extrapolated, or moving the upstream boundary to the leading edge of the plate where $u = u_\infty$ and v=0. These boundary conditions, however, were not as effective as the chosen conditions. Overall, Figures 9-11 show that the Proteus performance is very good for incompressible, turbulent flat plate flow.

Laminar Developing Pipe Flow

The Proteus calculations for incompressible laminar developing pipe flow are shown in Figures 12 and 13 compared with the experimental data of Reshotko.[14] For this test case, an average Mach number of approximately 0.1 was used, and Re_D, the Reynolds number based on the pipe diameter, was 100. The pipe length was set to 10 diameters, and a 51 axial by 21 radial grid was used. For the initial flow field, u =v = 0 and p = p_r, where p_r is the reference pressure which was set to standard sea level pressure. For the boundary conditions, the inlet and exit pressure were chosen to achieve a pressure drop calculated by pipe design formulas. For the remaining inlet boundary conditions, $\partial^2 u/\partial x^2 = 0$ and $\partial v/\partial x = 0$. The remaining exit conditions were $\partial u/\partial x = \partial v/\partial x = 0$. At the pipe wall, $\partial p/\partial r = 0$ and u = v = 0. The centerline boundary conditions were standard symmetry conditions such that $\partial p/\partial r = \partial u/\partial r = 0$ and v = 0.

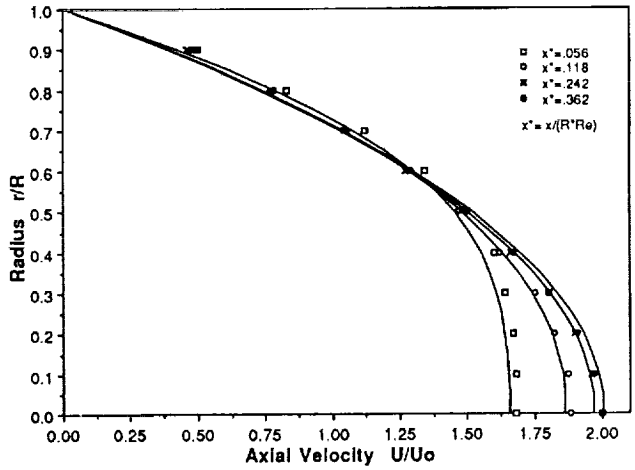

Fig. 12. Axial velocity profiles for laminar developing pipe flow.

In Figure 12, the nondimensionalized axial velocity, u/u_0, is plotted against the nondimensionalized radial position, r/R, with u_0 equal to the average velocity , r equal to the radial position in the pipe and R equal to the pipe radius. Results are plotted at various axial locations in the pipe, represented nondimensionally as $x/[(R)(Re_R)]$, with Re_R equal to the Reynolds number based on R. The Proteus results are shown as curves and the experimental data as symbols. As can be seen, the Proteus velocity profiles coincide fairly well with the experimental data and exhibit the distinctive bullet or Poisueille profile. Figure 13 represents the axial velocity in the pipe at selected radial positions. Again, the Proteus results are shown as curves and the experimental data as symbols. Here, the Proteus agreement is also good, but note that in both Figures 12 and 13, there is a slight deviance in the near-wall region where $r/R \approx 0.9$. Previous work has shown that this might be improved by packing more grid points near the wall to better resolve the steep gradients imposed by the no-slip wall boundary conditions. Overall, Proteus performs well for laminar developing pipe flows.

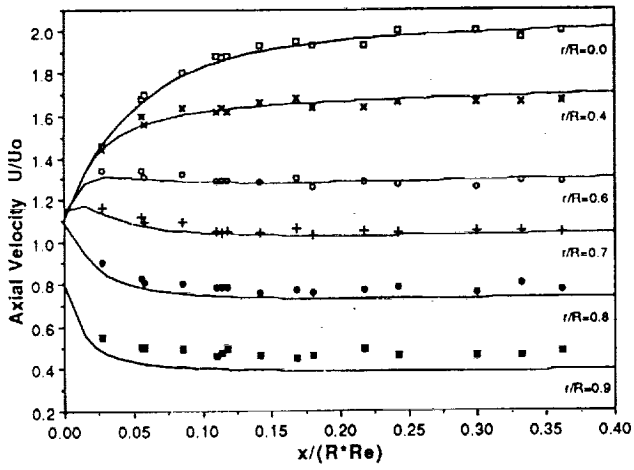

Fig. 13. Axial velocity profiles for laminar developing pipe flow.

Turbulent Developing Pipe Flow

The results for incompressible turbulent developing pipe flow are shown in Figures 14 and 15 compared with the experimental data of Barbin.[15] This case had an average Mach number of approximately 0.09 and Re_D=388,000. The pipe length was set to 50 diameters, and a 101 axial by 51 radial grid was used with a packing ratio of 0.05 near the wall. The initial and boundary conditions used were identical to those of the laminar developing pipe flow case.

Figures 14 and 15 show the Proteus results in a manner analogous to Figures 12 and 13 for laminar developing pipe flow. The value of u at the pipe inlet is approximately equal to the average velocity, u_0, which would be expected for turbulent developing pipe flow. Also, the Proteus results closely agree with the experimental data, with a slight deviation in the near-wall region. Thus, Proteus is capable of calculating turbulent developing pipe flows.

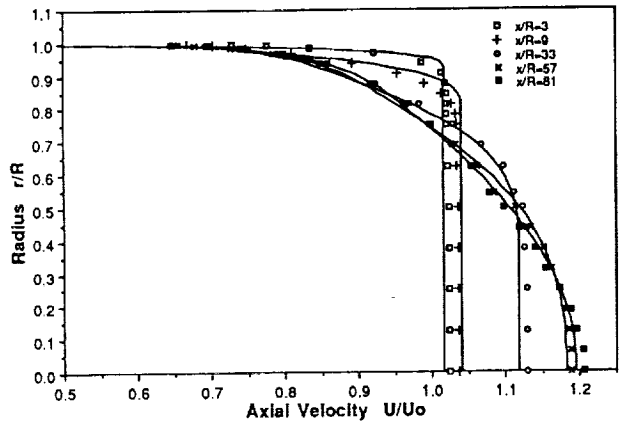

Fig. 14. Axial velocity profiles for turbulent developing pipe flow.

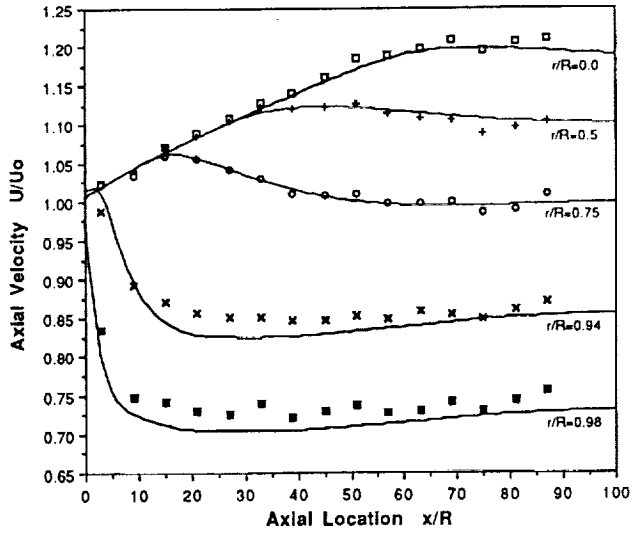

Fig. 15. Axial velocity profiles for turbulent developing pipe flow.

Swirling Developed Pipe Flow

In this validation case, the Proteus results for swirling incompressible turbulent pipe flow are compared with the experimental data of Weske.[16] The Mach number was 0.1 and Re_D=30,000. The pipe length was set to 50 diameters with a 400 axial by 50 radial grid, and a packing ratio of 0.1 near the wall. The initial conditions for u were calculated using the 1/7th power law, with the boundary layer thickness approximated as 10% of the pipe radius. The initial swirl velocity profile was linear with the swirl velocity w = 0 at the centerline and increasing to a maximum of $w = u_0$ near the wall, where u_0 is the centerline axial velocity for this case. This gives the swirl number of $\sigma = 1.0$, where $\sigma = w_{max}/u_0$. The remaining initial conditions were $p = p_r$, and v = 0. For the boundary conditions, the inlet and exit pressure were chosen so that the pressure drop coincided with the design pipe calculation value, ignoring the unknown effects of the swirling velocity component. The inlet velocities were held at the initial condition values and at the exit, $\partial u/\partial x = \partial v/\partial x = \partial w/\partial x = 0$. At the pipe wall, $\partial p/\partial r = 0$ and u = v = w = 0. At the centerline, $\partial p/\partial r = \partial u/\partial r = 0$ and v = w = 0.

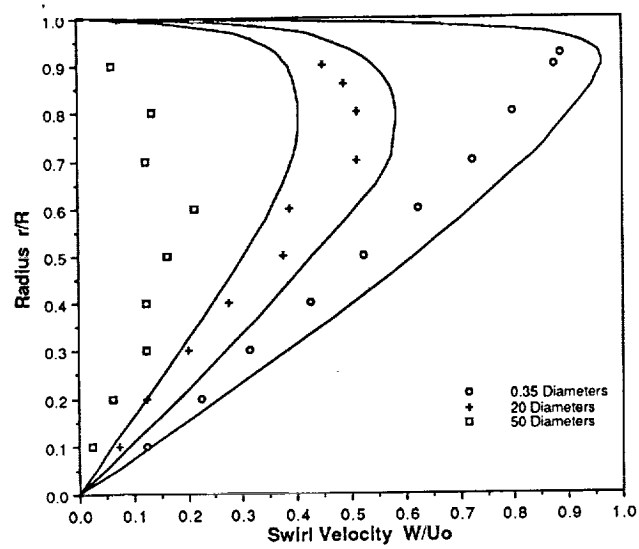

Fig. 16. Swirl velocity profiles in a pipe. (Inlet swirl number σ=1)

Figure 16 shows the Proteus swirl velocity profiles as curves and the experimental data as symbols. The plot shows a general agreement of the profile shape and swirl decay as the flow works its way down the pipe; however, the Proteus curves do not agree well with the data. The disagreement can be attributed to the inability of the algebraic eddy viscosity turbulence model to handle the anisotropies of this complex flow. Yoo et al.[17] describe the problems of computing the turbulence field for a similar flow.

Concluding Remarks

Validation cases for both laminar and turbulent incompressible flow over a flat plate at zero pressure gradient showed excellent agreement with exact solutions, empirical correlations and experimental data. It was also shown that a 26x51 grid with packing near the wall gives sufficient resolution to calculate laminar flat plate flow. The velocity profiles of both laminar and turbulent developing pipe flow agreed with experimental data, with slight deviations near the pipe wall. Pipe flow with a swirl number of 1.0 showed the expected profile shape and swirl decay; however, the swirl velocity profiles did not coincide with experimental data. This is a shortcoming of the algebraic eddy viscosity model used in Proteus for computing swirling pipe flows. With this exception, Proteus, is proven to be effective for calculating simple internal and external, incompressible, viscous flows.

Validation of Proteus is ongoing. Future plans include verification of higher Mach number flows and flows with heat transfer.

References

1. Towne, C. E., Schwab, J. R., Benson, T. J., and Suresh, A., "PROTEUS Two-Dimensional Navier-Stokes Computer Code -- Version 1.0, Vols. 1-3," NASA TM 102551-102553, March, 1990.

2. Baldwin, B. S., and Lomax, H., "Thin Layer Approximation and Algebraic Model for Separated Turbulent Flows," AIAA Paper 78-257, Jan. 1978.

3. Briley, W. R., and McDonald, H., "Solution of the Multidimensional Compressible Navier-Stokes Equations by a Generalized Implicit Methods," J. Comp. Phys., Vol. 24, Aug. 1977, pp. 373-397.

4. Beam, R. M., and Warming, R. F., "An Implicit Factored Scheme for the Compressible Navier-Stokes Equations," AIAA J., Vol. 16, April 1978, pp. 393-402.

5. Steger, J. L., "Implicit Finite-Difference Simulation of Flow about Arbitrary Two-Dimensional Geometries,"AIAA J., Vol. 16, July 1978, pp. 679-686.

6. Pulliam, T.H., "Artificial Dissipation Models for the Euler Equations," AIAA J., Vol. 24, Dec. 1986, pp. 1931-1940.

7. Jameson, A., Schmidt, W., and Turkel, E., "Numerical Solutions of the Euler Equations by Finite Volume Methods Using Runge-Kutta Time-Stepping Schemes," AIAA Paper 81-1259, 1981.

8. Schlicting, H., *Boundary Layer Theory,* McGraw-Hill Book Company, New York, 1968.

9. Musker, A. J.,"Explicit Expression for the Smooth Wall Velocity Distribution in a Turbulent Boundary Layer,"AIAA J. Vol. 17, No. 6, June 1979, pp. 655-657.

10. Klebanoff, P.S., "Characteristics of Turbulence in a Boundary Layer with Zero Pressure Gradient," NACA Report 1247, 1953.

11. White, F. M., *Viscous Fluid Flow,* McGraw-Hill, Inc., 1974.

12. Hopkins, E. J., and Inouye, M, "An Evaluation of Theories for Predicting Turbulent Skin Friction and Heat Transfer on Flat Plates at Supersonic and Hypersonic Mach Numbers," AIAA J.Vol. 9, No. 6, June, 1971, pp. 993-1003.

13. Weighardt, K., "Flat Plate Flow. u_∞ = 33 m/sec", AFOSR-IFP-Stanford Conference on Computation of Turbulent Boundary Layers-1968", Vol. II, Ed. by Coles, D.E. and Hirst, E.A., 1968.

14. Reshotko, E., "Experimental Study of the Stability of Pipe Flow, I. Establishment of an Axially Symmetric Poisueille Flow," Progress Report No. 20-354, Department of the Army Ordinance Corps, October, 1958.

15. Barbin, A. R., "Development of Turbulence in the Inlet of a Smooth Pipe," Ph.D. Thesis, Purdue Univ., 1961.

16. Weske, D. R., "Experimental Study of Turbulent Swirled Flows in a Cylindrical Tube," *Fluid Mechanics -- Soviet Research,* Vol. 3, No. 1, Jan.-Feb., 1974, pp. 77-82.

17. Yoo, G. J., So, R. M. C., and Hwang, B. C., "Calculation of Developing Turbulent Flows in a Rotating Pipe," *ASME J. of Turbomachinary,* Vol. 113, January 1991, pp. 34-41.

REPORT DOCUMENTATION PAGE

Form Approved
OMB No. 0704-0188

1. AGENCY USE ONLY (*Leave blank*)	2. REPORT DATE	3. REPORT TYPE AND DATES COVERED
		Technical Memorandum

4. TITLE AND SUBTITLE

Verification of the Proteus Two-Dimensional Navier-Stokes Code for Flat Plate and Pipe Flows

5. FUNDING NUMBERS

WU-505-62-21

6. AUTHOR(S)

Julianne M. Conley and Patrick L. Zeman

7. PERFORMING ORGANIZATION NAME(S) AND ADDRESS(ES)

National Aeronautics and Space Administration
Lewis Research Center
Cleveland, Ohio 44135-3191

8. PERFORMING ORGANIZATION REPORT NUMBER

E-6449

9. SPONSORING/MONITORING AGENCY NAMES(S) AND ADDRESS(ES)

National Aeronautics and Space Administration
Washington, D.C. 20546-0001

10. SPONSORING/MONITORING AGENCY REPORT NUMBER

NASA TM-105160
AIAA-91-2013

11. SUPPLEMENTARY NOTES

Prepared for the 27th Joint Propulsion Conference cosponsored by AIAA, SAE, ASME, and ASEE, Sacramento, California, June 24-27, 1991. Julianne M. Conley, NASA Lewis Research Center; Patrick L. Zeman, Arnold Engineering and Development Center, Arnold AFB, Tennessee. Responsible person, Julianne M. Conley, (216) 433-2188.

12a. DISTRIBUTION/AVAILABILITY STATEMENT

Unclassified - Unlimited
Subject Category 34

12b. DISTRIBUTION CODE

13. ABSTRACT (*Maximum 200 words*)

The Proteus Navier-Stokes Code is evaluated for two-dimensional/axisymmetric, viscous, incompressible, internal and external flows. The particular cases to be discussed are laminar and turbulent flows over a flat plate, laminar and turbulent developing pipe flows and turbulent pipe flow with swirl. Results are compared with exact solutions, empirical correlations and experimental data. A detailed description of the code set-up, including boundary conditions, initial conditions, grid size and grid packing is given for each case.

14. SUBJECT TERMS

Navier-stokes equation; Two-dimensional flow; Axisymmetric flow; Laminar flow; Turbulent flow; Flat plates; Boundary layer flow; Pipe flow; Swirling

15. NUMBER OF PAGES

8

16. PRICE CODE

A02

17. SECURITY CLASSIFICATION OF REPORT	18. SECURITY CLASSIFICATION OF THIS PAGE	19. SECURITY CLASSIFICATION OF ABSTRACT	20. LIMITATION OF ABSTRACT
Unclassified	Unclassified	Unclassified	